Radiative corrections to elastic muon-proton scattering at low momentum transfers

Norbert Kaiser[*]

Physik-Department T39, Technische Universität München, D-85748 Garching, Germany

Yong-Hui Lin[†]

*Helmholtz-Institut für Strahlen- und Kernphysik and Bethe Center for Theoretical Physics,
Universität Bonn, D-53115 Bonn, Germany*

Ulf-G. Meißner[‡]

*Helmholtz-Institut für Strahlen- und Kernphysik and Bethe Center for Theoretical Physics,
Universität Bonn, D-53115 Bonn, Germany and Institute for Advanced Simulation, Institut für Kernphysik,
Center for Advanced Simulation and Analytics, and Jülich Center for Hadron Physics,
Forschungszentrum Jülich, D-52425 Jülich, Germany*

We systematically calculate the radiative corrections of order α/π to elastic muon-proton scattering at low momentum transfers. These include vacuum polarization, photon-loop form factors of the muon and the proton, two-photon exchange corrections and soft photon radiation. In particular, we discuss these corrections for the kinematics of the upcoming AMBER experiment with a 100 GeV muon beam. It is found that for the ratio to the Born cross section, only the minor terms from the photon-loop form factors of the proton and two-photon exchange depend on the proton structure as predetermined by the strong interactions. The inclusion of soft photon radiation (below 20 MeV), which as such is mandatory to cancel the infrared divergences arising from virtual photon loops, points to a prominent role of bremsstrahlung among the radiative corrections of order α/π. Therefore, the calculation of the process $\mu^\mp p \to \mu^\mp p \gamma$ must be extended beyond the soft photon approximation and tailored to the specific experimental conditions for a proper analysis of the upcoming AMBER data.

I. INTRODUCTION

Elastic muon-proton scattering at low momentum transfers offers an alternative method to measure the proton charge radius r_p, which is a fundamental quantity in the theory of the strong interactions. It is defined here by the slope of the proton electric form factor $G_{E,p}(Q)$ at zero momentum transfer $r_p^2 = -6dG_{E,p}(Q)/dQ^2|_{Q=0}$, with Q^2 the invariant four-momentum transfer squared. Any deviation from the value measured in electron-proton scattering would challenge the concept of lepton-flavor universality, which is a cornerstone of the so successful Standard Model of particle physics, that has been challenged in recent experiments on certain decay modes of B mesons; see Ref. [1] for a recent review. Two experiments are pursuing such proton radius measurements, namely MUSE at PSI [2] and AMBER at CERN [3]. Both experiments were triggered by the so-called "proton radius puzzle;" see e.g. Ref. [4], but it must be said that most recent determinations of the proton radius from electron-proton scattering and the Lamb shift in electronic hydrogen are in favor of the so-called small radius, $r_p \simeq 0.84$ fm, as collected in Table I. The small value is further supported by a dispersion-theoretical analysis of all existing scattering and annihilation data in the spacelike and the timelike region [5], as also shown in the table. The underlying dispersive framework and the history of proton radius extractions based on dispersion relations (DRs) are discussed in detail in Ref. [6]. Still, an independent extraction from $\mu^\mp p$ scattering would be highly welcome, further complementing the groundbreaking work on the Lamb shift in muonic hydrogen [7], which essentially initiated the whole proton radius discussion.

[*]nkaiser@ph.tum.de
[†]yonghui@hiskp.uni-bonn.de
[‡]meissner@hiskp.uni-bonn.de

TABLE I. Modern precision extractions of the proton charge radius r_p from the Lamb shift in electronic hydrogen and electron-proton scattering as well as dispersion theory.

r_p (fm)	Year	Method	References
0.877(13)	2018	H Lamb shift	[8]
0.833(10)	2019	H Lamb shift	[9]
0.8482(38)	2020	H Lamb shift	[10]
0.8584(51)	2021	H Lamb shift	[11]
0.831(7)(12)	2019	ep scattering	[12]
0.840(3)(2)	2022	Dispersion theory	[5]

In this work we consider the radiative corrections to $\mu^{\mp} p$ scattering specifically for the kinematics of the AMBER experiment, which operates with a high-energetic muon beam at 100 GeV and measures in near-forward directions, thus spanning the momentum transfers 32 MeV $<$ $Q <$ 141 MeV, which nicely overlaps with the range of the upcoming MUSE experiment at PSI with 45 MeV $<$ $Q <$ 265 MeV, the PRAD-II experiment at Jefferson Lab for $e^- p$ scattering with 14 MeV $< Q <$ 245 MeV [13] as well as the MAGIC $e^- p$ experiment at Mainz, that aims at a momentum range 10 MeV $< Q <$ 292 MeV [14]. The AMBER experiment intends to measure the proton radius with an accuracy of better than 0.01 fm, which requires a detailed study of the radiative corrections to be able to achieve such an accuracy. Such a calculation is provided here, based on the works in Refs. [15,16] employing the best phenomenological available proton form factors from Ref. [5]. For related work on radiative corrections to muon-proton scattering, see Refs. [17–20].

The manuscript is organized as follows: In Sec. II we display the differential cross section for $\mu^- p$ scattering including the various radiative correction terms. These are discussed in detail in the following sections, namely the photon-loop form factors of the muon and of the proton in Sec. III, the two-photon corrections in Sec. IV and the soft-photon radiation in Sec. V. Finally, in Sec. VI, we put all pieces together and display and discuss the radiative corrections for the AMBER kinematics, adding for comparison the analogous results for the MUSE kinematics. We end with a short summary and an outlook in Sec. VII.

II. DIFFERENTIAL CROSS SECTION

We consider elastic muon scattering off protons, specifically the process $\mu^-(k_1) + p(p_1) \to \mu^-(k_2) + p(p_2)$, and introduce the dimensionless Mandelstam variables:

$$s = (p_1 + k_1)^2 / M^2, \quad t = (k_1 - k_2)^2 / M^2, \quad u = (p_1 - k_2) / M^2, \tag{1}$$

that satisfy the constraint $s + t + u = 2 + 2r$, with $M = 938.272$ MeV the proton mass and the squared muon-to-proton mass ratio $r = (m_\mu/M)^2 = 1.2681 \times 10^{-2}$. The

advantage of these (uncommon) dimensionless variables (s, t, u) is that they allow us to write the differential cross-section and radiative corrections in concise analytical form without repeating permanently the mass parameters.

The unpolarized differential cross section for $\mu^- p \to \mu^- p$ including radiative corrections of order α/π, with $\alpha = 1/137.036$ the electromagnetic fine-structure constant, reads

$$\frac{d\sigma}{dt} = \frac{4\pi\alpha^2}{M^2 t^2 P} \{ H_0(1 + 2\Pi_{\text{vp}} + \delta_{\text{soft}}) + H_1 + H_2 \}, \tag{2}$$

where the polynomial $P = s^2 - 2s(1 + r) + (1 - r)^2$ is equal to the Källén function $\lambda(s, 1, r)$. The first term proportional to H_0 gives the Rosenbluth formula, generalized by the inclusion of the finite lepton mass, and reads

$$H_0 = \left[\frac{(s + 1 - r)^2}{4 - t} + r - s \right] (4G_E^2 - tG_M^2) + t\left(r + \frac{t}{2} \right) G_M^2. \tag{3}$$

The argument $Q = \sqrt{-t} M$ of the proton electric and magnetic form factors $G_E(Q)$ and $G_M(Q)$, respectively, that arise from the nonperturbative strong interactions, is not displayed explicitly. The second term in Eq. (2) describes vacuum polarization in the one-photon exchange through the Q-dependent function Π_{vp}. For the low momentum transfers considered in this work, vacuum polarization due to the two lightest leptons is sufficient:

$$\Pi_{\text{vp}} = \frac{\alpha}{3\pi} \sum_{e,\mu} \left[\frac{1}{\tau^2} - \frac{5}{3} + \frac{2\tau^2 - 1}{\tau^3} \sqrt{1 + \tau^2} \ln(\tau + \sqrt{1 + \tau^2}) \right], \tag{4}$$

where $\tau_e = Q/2m_e$ and $\tau_\mu = Q/2m_\mu$. At $Q = 300$ MeV one gets $\Pi_{\text{vp}} = (0.86 + 0.07)\% = 0.93\%$, and at $Q = 100$ MeV one has $\Pi_{\text{vp}} = (0.69 + 0.01)\% = 0.70\%$. These numbers demonstrate the dominance of electronic vacuum polarization. Further features are illustrated in Fig. 82 of Ref. [21], which shows the quantity $|1 + \Pi_{\text{vp}}|^2$ in the spacelike and timelike regions below 2 GeV and thereby delineates the region, where leptonic vacuum polarization is actually dominant.

The next correction factor δ_{soft} arises from soft photon bremsstrahlung and its derivation will be outlined in Sec. V, starting from the basic soft photon amplitude. Moreover, the term proportional to H_1 in Eq. (2) gives twice the interference term of one-photon exchange with electromagnetic vertex corrections at the muon and at the proton. It is given by the expression

$$H_1 = 2F_1^\gamma H_0 + F_2^\gamma t(2G_E^2 + tG_M^2)$$
$$+ 8G_E^\gamma \left[\frac{(s+1-r)^2}{4-t} + r - s \right] G_E$$
$$+ G_M^\gamma \left[2s + t - \frac{2(s+1-r)^2}{4-t} \right] tG_M, \qquad (5)$$

where $F_{1,2}^\gamma$ denote the photon-loop form factors of the muon and $G_{E,M}^\gamma$ are those of the proton. These quantities are discussed in some detail in Sec. III.

Finally, the last piece proportional to H_2 in Eq. (2) gives twice the interference term of one-photon exchange with the planar and crossed two-photon exchange box diagrams; see Sec. IV. Note that H_0 and H_1 are even under $s \leftrightarrow u$, while H_2 is odd. The differential cross section for the process $\mu^+(k_1) + p(p_1) \rightarrow \mu^+(k_2) + p(p_2)$ is thus obtained by $s \leftrightarrow u$ crossing of the terms in the curly brackets of Eq. (2), i.e., one merely has to change the sign of H_2.

III. PHOTON-LOOP FORM FACTORS OF MUON AND PROTON

In this section, we discuss the photon-loop form factors of the muon and of the proton that appear in the expression
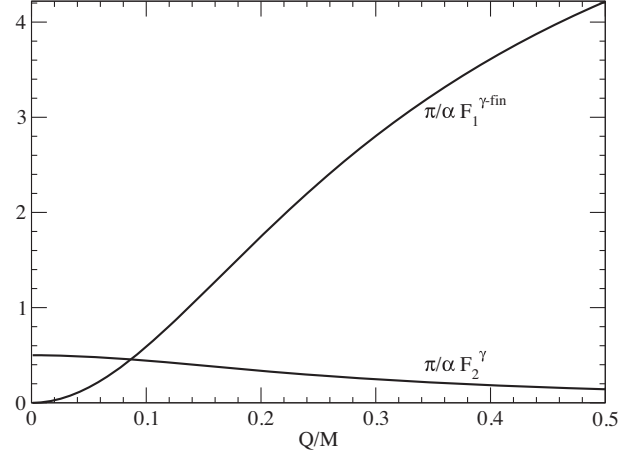

FIG. 1. Photon-loop form factors $F_{1,2}^\gamma$ of the muon, where $F_1^{\gamma\text{-fin}}$ refers to the infrared-finite part.

for H_1; see Eq. (5). The photon-loop form factors of the muon are obtained from a standard QED calculation of the triangle diagram (and self-energy diagram which contributes through the muon wave-function renormalization factor Z_2) and they explicitly read

$$F_1^\gamma = \frac{\alpha t}{2\pi} \int_4^\infty dx \, \frac{1}{x(xr-t)\sqrt{x^2-4x}} \left\{ [2\xi_{\text{ir}} + \ln r + \ln(x-4)](x-2) + 4 - \frac{3x}{2} \right\}$$
$$= \frac{\alpha}{\pi} \left\{ (2\xi_{\text{ir}} + \ln r) \left(\frac{1}{2} + \frac{t-2r}{\sqrt{t^2-4rt}} \ln \frac{\sqrt{4r-t}+\sqrt{-t}}{2\sqrt{r}} \right) + \frac{(2r-t)}{\sqrt{t^2-4rt}} \left[\ln^2 \frac{\sqrt{4r-t}+\sqrt{-t}}{2\sqrt{r}} \right. \right.$$
$$+ \left(\frac{8r-3t}{4r-2t} - \ln \frac{4r-t}{r} \right) \ln \frac{\sqrt{4r-t}+\sqrt{-t}}{2\sqrt{r}} + \text{Li}_2 \left(\frac{t-2r+\sqrt{t^2-4rt}}{2r} \right) + \frac{\pi^2}{12} \right] - 1 \left. \right\}, \qquad (6)$$

$$F_2^\gamma = \frac{2\alpha}{\pi} \frac{r}{\sqrt{t^2-4rt}} \ln \frac{\sqrt{4r-t}+\sqrt{-t}}{2\sqrt{r}}. \qquad (7)$$

$$G_{E,M}^\gamma = \frac{\alpha}{\pi} \xi_{\text{ir}} \left(1 + \frac{2t-4}{\sqrt{t^2-4t}} \ln \frac{\sqrt{4-t}+\sqrt{-t}}{2} \right) G_{E,M}$$
$$+ G_{E,M}^{\gamma\text{-fin}} + G_{E,M}^{\gamma\Delta} + G_{E,M}^{\gamma\Delta\Delta}, \qquad (8)$$

The infrared divergence ξ_{ir} is defined as $\xi_{\text{ir}} = \ln(M/m_\gamma)$, with m_γ an infinitesimal regulator photon mass. Moreover, $\text{Li}_2(a) = a \int_1^\infty dx [x(x-a)]^{-1} \ln x$ denotes the conventional dilogarithmic function for $a < 1$. One observes that the $F_{1,2}^\gamma$ are actually functions of the ratio $-t/r$ and the first version of F_1^γ is a once-subtracted dispersion relation. Note that $F_1^\gamma(0) = 0$ and $F_2^\gamma(0) = \alpha/2\pi = 1.1614 \times 10^{-3}$ gives the leading correction to the muon anomalous magnetic moment. These form factors are shown (multiplied with π/α) in Fig. 1, leaving out the regularization-dependent ξ_{ir} term for F_1^γ.

The photon-loop form factors of the proton are composed in a similar way of infrared-divergent and infrared-finite pieces:

where $G_{E,M}^{\gamma\text{-fin}}$ denotes the infrared-finite part and $G_{E,M}^{\gamma\Delta} + G_{E,M}^{\gamma\Delta\Delta}$ arises from treating inelastic contributions through single and double $\Delta^+(1232)$ resonance excitation of the proton.

The contributions to $G_{E,M}^{\gamma\text{-fin}}$ from the triangle diagram in Fig. 2 can be calculated numerically as double integrals $\frac{\alpha}{\pi} \int_0^\infty dx \int_{-1}^{+1} dz \sqrt{1-z^2} \{[...]G_E(Q) + [...]G_M(Q)\}$ over cubic expressions in some given phenomenological form factors $G_{E,M}$. The proton form factors enter linearly in the external momentum transfer Q and quadratically in the loop-momentum xM inside the square brackets. The wave-function renormalization factor Z_2 from the self-energy diagram (see right part of Fig. 2) must also be taken into account in order to ensure that $G_E^\gamma(0) = 0$. Using the
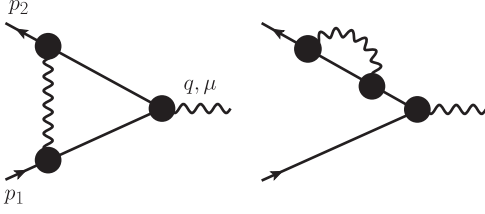
FIG. 2. Photonic vertex and self-energy corrections with proton intermediate states.

representation of Z_2 in terms of an integral over the proton form factors as written in Eq. (5) of Ref. [16], one gets $Z_2 = \frac{\alpha}{\pi}\xi_{\mathrm{ir}} + Z_2^{\mathrm{fin}}$, where $Z_2^{\mathrm{fin}} \simeq -2.1\alpha/\pi$ depends weakly on the choice of proton form factors $G_{E,M}$.

In this work we model inelastic contributions to the photon-loop form factors of the proton by single and double excitation of the $\Delta^+(1232)$ resonance, as shown in Fig. 3. As we will see later, this is appropriate here. More sophisticated approaches could also be entertained, see e.g. the review [22], but we refrain from doing so here. The Lorentz-covariant description of the spin-3/2 Δ isobar requires a Rarita-Schwinger spinor Ψ_α. We use a minimal gauge-invariant form of the $\Delta^+ p\gamma$ vertex:

$$\frac{ie\kappa^*}{\sqrt{6}M}(g^{\mu\alpha}\gamma\cdot q - \gamma^\mu q^\alpha)\gamma_5 G_\Delta(\sqrt{-q^2}), \qquad (9)$$

in terms of the transition magnetic moment $\kappa^* \simeq 5.0$ and a phenomenological transition form factor

$$G_\Delta(Q) = \left(1 + \frac{Q^2}{\Lambda^2}\right)^{-2}\exp\left(-\frac{Q^2}{7\Lambda^2}\right), \qquad (10)$$

with dipole mass $\Lambda = 843$ MeV, as extracted from pion electroproduction in the Δ-resonance region [23–25]. Here, q denotes the spacelike four-momentum carried by the virtual photon, so that $Q = \sqrt{-q^2}$. A commonly used form of the Rarita-Schwinger propagator (from index β to index α) reads

$$\frac{i}{3}\frac{\gamma\cdot p + M_\Delta}{M_\Delta^2 - p^2}\left(3g_{\alpha\beta} - \gamma_\alpha\gamma_\beta - \frac{2p_\alpha p_\beta}{M_\Delta^2} + \frac{p_\alpha\gamma_\beta - \gamma_\alpha p_\beta}{M_\Delta}\right), \qquad (11)$$
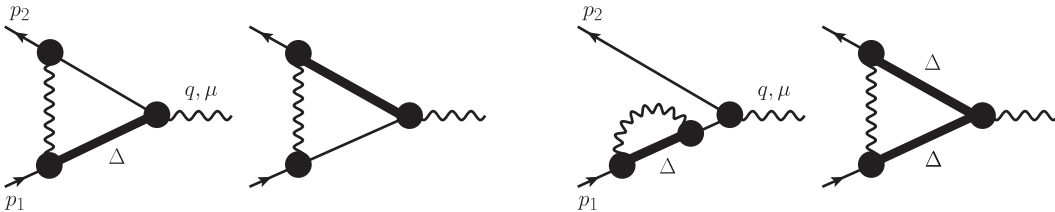
with p the four-momentum of the propagating Δ isobar. The left two diagrams in Fig. 3 provide equal contributions to $G_{E,M}^{\gamma\Delta}$, respectively, and the condition $G_E^{\gamma\Delta}(0) = 0$ follows immediately from the magnetic coupling vertex in Eq. (9). In order to evaluate the right diagram in Fig. 3, the $\Delta^+\Delta^+\gamma$ vertex is needed. It is naturally obtained by gauging the kinetic term of the free Rarita-Schwinger Lagrangian [26] as

$$ie(-\gamma^\mu g_{\alpha\beta} + \gamma_\alpha g_\beta^\mu + \gamma_\beta g_\alpha^\mu - \gamma_\alpha\gamma^\mu\gamma_\beta), \qquad (12)$$

with β the incoming and α the outgoing (Rarita-Schwinger) index. Further, we multiply this electric vertex with a dipole form factor times a (squared) exponential function as in Eq. (10). The third diagram in Fig. 3 contributes as $Z_2^{(\Delta)}G_{E,M}$, with the wave-function renormalization factor $Z_2^{(\Delta)} \simeq 0.273\alpha/\pi$, whose formula is written in Eq. (16) of Ref. [16]. It is worth to mention that only the combination of both right diagrams ensures the condition $G_E^{\gamma\Delta\Delta}(0) = 0$ for the photon-loop induced electric form factor. The various contributions to the photon-loop proton form factors multiplied with π/α are shown in Fig. 4, for two choices of proton form factors, namely the well-known (simple) dipole form and the most recent parametrization based on dispersion theory, that describe essentially all data in the timelike and in the spacelike regions [5]. We note that there are cancellations between the single- and the double-Δ contributions to both form factors, and that only the Δ contribution to the magnetic form factor is sizable (on the scale of $\alpha/\pi = 2.323 \times 10^{-3}$). Although the curve for $G_E^{\gamma\text{-fin}}$ shown in Fig. 4 appears to drop linearly for small Q, the underlying analytical expression is manifestly even under $Q \to -Q$, and this is true for any form factor.

IV. TWO-PHOTON EXCHANGE BOX DIAGRAMS

We now consider the two-photon exchange correction incorporated in the H_2 term. For a pointlike proton with $G_E = G_M = 1$ the ratio H_2/H_0 can be inferred from the calculation in Sec. 3 of Ref. [15] as

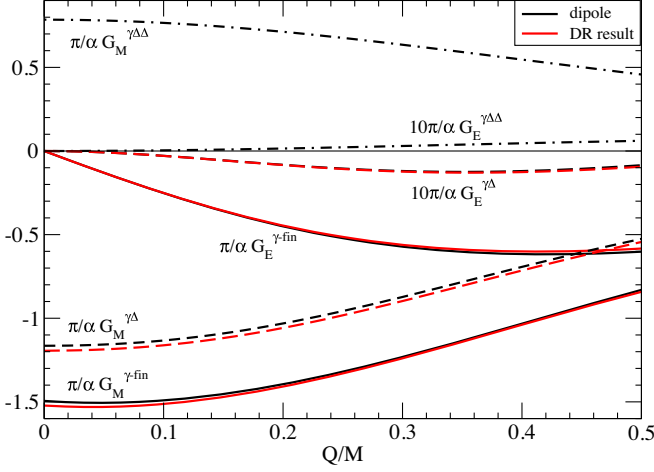FIG. 3. Photonic vertex and self-energy corrections with $\Delta^+(1232)$ intermediate states.

FIG. 4. Various contributions to the electric and magnetic photon-loop form factors of the proton. The black lines represent results obtained by using the dipole parametrization and the red lines show the calculations based on the form factors from Ref. [5].

$$\frac{H_2}{H_0} = -\frac{2t}{A' \otimes A'} \mathrm{Re}(\mathrm{III}' \otimes A' + \mathrm{IV}' \otimes A'), \quad (13)$$

where the change of sign is necessary, because there the case of equally charged leptons of different masses has been considered. The pertinent one-photon exchange term is $A' \otimes A' = 2(s - 1 - r)^2 + 2st + t^2$ and $\mathrm{III}' \otimes A'$ is written in Eq. (31) of Ref. [15], while $\mathrm{IV}' \otimes A' = -\mathrm{III}' \otimes A'|_{s \to u}$.
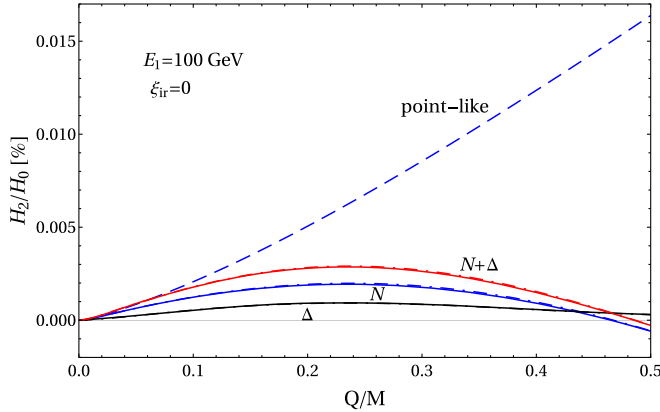

FIG. 5. The ratio H_2/H_0 for a pointlike proton (dashed line) and for the physical proton (line labeled "$N + \Delta$"). The elastic contribution and the inelastic contribution (modeled by single Δ-isobar excitation) are shown separately by the lines labeled "N" and "Δ." Solid lines refer to the use of the form factors from Ref. [5] and dotted-dashed lines are based on dipole form factors.

For a structureless proton the ratio H_2/H_0 (setting $\xi_{\mathrm{ir}} = 0$) at the AMBER kinematics ($E_1 = 100$ GeV or $s \simeq 214$) is found to be rather small, starting from zero at $Q = 0$ and increasing to about 0.016% at $Q = M/2 = 469$ MeV; see Fig. 5. This small value results from a strong cancellation between the planar and crossed 2γ-exchange box graph, namely 7.743%–7.727%. In the limit $Q \to 0$, where the cancellation becomes exact, the contributions from the planar and crossed box graph behave each as $\xi_{\mathrm{ir}} + \ln(Q/M)$ times an (r, s)-dependent factor of opposite sign. As also shown in Fig. 5, this cancellation is even more pronounced for the physical proton. For the nucleon intermediate state, we use the Feynman graph formalism of Ref. [27], representing the proton form factors as a sum of monopoles, and the Δ^+ intermediate state is evaluated using the dispersion relation approach of Refs. [28,29] in an approximation that neglects quadratic terms in the muon-to-proton mass ratio. The ratio H_2/H_0 does not exceed the value 0.003% for the low momentum transfers considered here.

V. SOFT PHOTON RADIATION

Without the inclusion of the soft photon radiation the treatment of radiative corrections to $\mu^- p \to \mu^- p$ is incomplete or even meaningless. When working at higher order in the electromagnetic coupling e, the muon and proton can radiate a real photon with four-momentum ℓ and polarization vector ϵ in the initial or final state, as shown in Fig. 6. The corresponding soft amplitude reads

$$e\left(\frac{\epsilon \cdot k_1}{\ell \cdot k_1} - \frac{\epsilon \cdot k_2}{\ell \cdot k_2} - \frac{\epsilon \cdot p_1}{\ell \cdot p_1} + \frac{\epsilon \cdot p_2}{\ell \cdot p_2}\right), \quad (14)$$

where the soft momentum ℓ is neglected in the numerator, and the accompanying $\mu^- p \to \mu^- p$ process is kept in the limit $\ell = 0$. Note that the signs in Eq. (14) indicate the charge of the radiating particle and whether this emission happens in the initial or the final state. The soft amplitude gets squared and summed over the two transversal polarizations by employing $\sum_{pol} \epsilon^\mu \epsilon^\nu = -g^{\mu\nu}$, which leads to
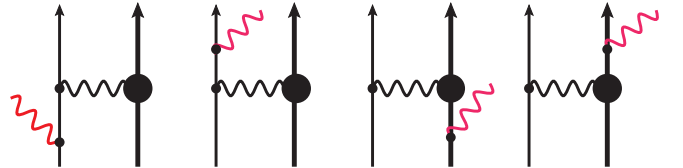

FIG. 6. Diagrams representing the four amplitudes for soft photon radiation. Thin and solid lines denote muons and protons, respectively, while the wiggly lines denote photons. The corresponding (pointlike and structureful) vertices are depicted by small and large filled circles.

$$4\pi\alpha\left\{-\frac{m_\mu^2}{(\ell\cdot k_1)^2}-\frac{m_\mu^2}{(\ell\cdot k_2)^2}-\frac{M^2}{(\ell\cdot p_1)^2}-\frac{M^2}{(\ell\cdot p_2)^2}\right.$$
$$\left.+\frac{2k_1\cdot k_2}{\ell\cdot k_1\ell\cdot k_2}+\frac{2p_1\cdot p_2}{\ell\cdot p_1\ell\cdot p_2}+\frac{2k_1\cdot p_1}{\ell\cdot k_1\ell\cdot p_1}+\frac{2k_2\cdot p_2}{\ell\cdot k_2\ell\cdot p_2}-\frac{2k_1\cdot p_2}{\ell\cdot k_1\ell\cdot p_2}-\frac{2k_2\cdot p_1}{\ell\cdot k_2\ell\cdot p_1}\right\}. \quad (15)$$

In any experiment with finite energy resolution, the emission of additional soft photons with $|\vec{\ell}|<\lambda$ is undetectable and thus gets subsumed in the cross section for the elastic scattering process. The integrals of the ten terms in Eq. (15) over a (small) momentum sphere $|\vec{\ell}|<\lambda$ are solved with the help of the following (infrared-regularized) master integral:

$$\int_0^\lambda d\ell\frac{\ell^2}{2\sqrt{m_\gamma^2+\ell^2}}\int_{-1}^{+1}dz\frac{-1}{(E\sqrt{m_\gamma^2+\ell^2}-p\ell z)^2}=\frac{1}{E^2-p^2}\left[\ln\frac{m_\gamma}{2\lambda}+\frac{E}{2p}\ln\frac{E+p}{E-p}\right]. \quad (16)$$

It applies directly to the first four terms in Eq. (15) with squares in the denominator, whereas for the six terms with products in the denominator one makes use of the Feynman parametrization: $(AB)^{-1}=\int_0^1 dx[Ax+B(1-x)]^{-2}$. Putting all pieces together, the correction factor from soft photon radiation is given by the sum $\delta_{\text{soft}}=\delta_{\text{soft}}^{(\text{uni})}+\delta_{\text{soft}}^{(\text{cm})}$, where the universal part reads

$$\delta_{\text{soft}}^{(\text{uni})}=\frac{4\alpha}{\pi}\left(\ln\frac{M}{2\lambda}-\xi_{\text{ir}}\right)\left\{1+\frac{t-2r}{\sqrt{t^2-4rt}}\ln\frac{\sqrt{4r-t}+\sqrt{-t}}{2\sqrt{r}}+\frac{t-2}{\sqrt{t^2-4t}}\ln\frac{\sqrt{4-t}+\sqrt{-t}}{2}\right.$$
$$\left.+\frac{2(1+r-s)}{\sqrt{s-\rho_+}\sqrt{s-\rho_-}}\ln\frac{\sqrt{s-\rho_+}+\sqrt{s-\rho_-}}{2r^{1/4}}+\frac{2(1+r-u)}{\sqrt{\rho_+-u}\sqrt{\rho_--u}}\ln\frac{\sqrt{\rho_+-u}+\sqrt{\rho_--u}}{2r^{1/4}}\right\}, \quad (17)$$

with $\rho_\pm=1+r\pm 2\sqrt{r}$. It cancels exactly the infrared divergences proportional to ξ_{ir} from the virtual photon loops and the remainder depends logarithmically on an infrared cutoff λ for undetected soft photon radiation. Note that the last two terms cancel the infrared divergences from the two-photon exchange box diagrams. For these the antisymmetry under $s\leftrightarrow u$ is manifest by setting $\sqrt{u-\rho_\pm}=i\sqrt{\rho_\pm-u}$, $\sqrt{\rho_\pm-s}=i\sqrt{s-\rho_\pm}$ and taking eventually the real part of a logarithm. In the limit $r\to 0$ the sum of these two terms simplifies drastically to $\ln(1-u)-\ln(s-1)$. For $\mu^+p\to\mu^+p$ the last two terms in Eq. (17) change sign, keeping the role of s and u.

The other part of δ_{soft} is specific for assuming in the center-of-mass frame a small momentum sphere $|\vec{\ell}|<\lambda$ for undetected soft bremsstrahlung:

$$\delta_{\text{soft}}^{(\text{cm})}=\frac{\alpha}{\pi}\left\{\frac{2}{\sqrt{P}}\left[(s-1+r)\ln\frac{s-1+r+\sqrt{P}}{2\sqrt{sr}}+(s+1-r)\ln\frac{s+1-r+\sqrt{P}}{2\sqrt{s}}\right]\right.$$
$$+\int_0^{1/2}dx\left[\frac{(t-2r)(s-1+r)}{[r-tx(1-x)]\sqrt{R_t}}\ln\frac{s-1+r+\sqrt{R_t}}{s-1+r-\sqrt{R_t}}+\frac{(t-2)(s+1-r)}{[1-tx(1-x)]\sqrt{R_t}}\ln\frac{s+1-r+\sqrt{R_t}}{s+1-r-\sqrt{R_t}}\right]$$
$$+\int_0^1 dx\left[\frac{(1+r-s)[s+(1-r)(1-2x)]}{(1-2x)[sx(1-x)+(1-2x)(1-x-rx)]\sqrt{P}}\ln\frac{s+(1-2x)(1-r+\sqrt{P})}{s+(1-2x)(1-r-\sqrt{P})}\right.$$
$$\left.\left.+\frac{(1+r-u)[s+(1-r)(1-2x)]}{[1+(r-1)x-ux(1-x)]\sqrt{R_u}}\ln\frac{s+(1-r)(1-2x)+\sqrt{R_u}}{s+(1-r)(1-2x)-\sqrt{R_u}}\right]\right\}, \quad (18)$$

introducing the auxiliary polynomials $R_t=P+4stx(1-x)$ and $R_u=P+4x(1-x)[su-(1-r)^2]$, with $P=s^2-2s(1+r)+(1-r)^2$. Although possible, we refrain from solving the Feynman-parameter integrals in Eq. (18) which lead to overly complicated expressions involving squared logarithms and dilogarithms (see e.g. Eqs. (4.10)–(4.12) in Ref. [30]). For $\mu^+p\to\mu^+p$ the last term $\int_0^1 dx...$ changes sign, keeping the role of s and u.

VI. RESULTS AND DISCUSSION

We can now put the pieces together and discuss the radiative corrections to muon-proton scattering. First, it is interesting to see how much the radiative corrections to $\mu^-p\to\mu^-p$ scattering (at a beam energy of $E_1=100$ GeV) are affected by the underlying proton structure. For that purpose we make comparisons with a structureless proton, corresponding to $G_{E,M}=1$. Returning
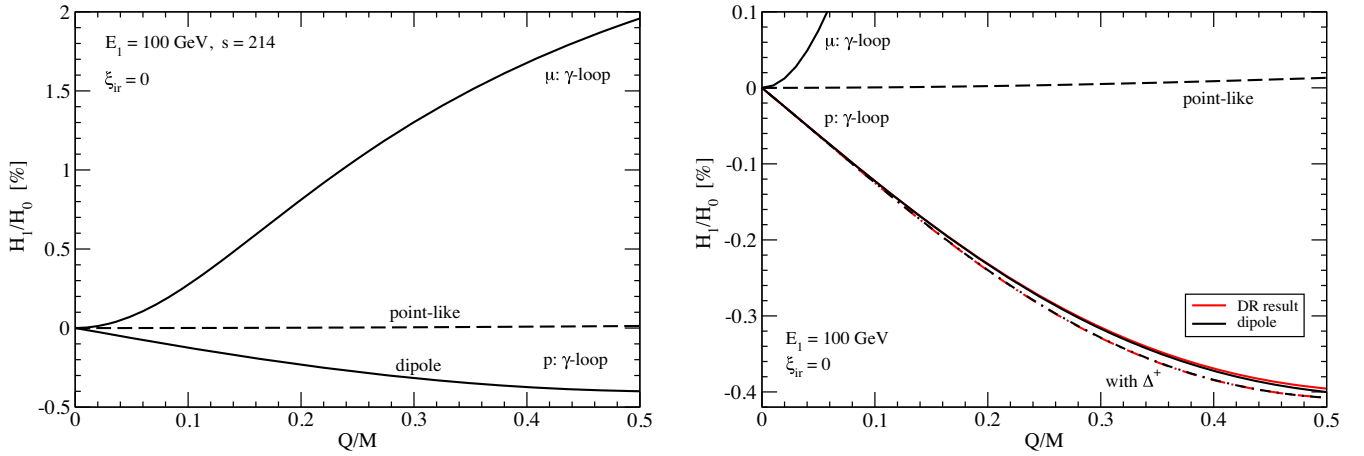
FIG. 7. Ratio H_1/H_0 due to electromagnetic vertex corrections separated into parts from the muon and the proton. Left panel: Corrections from the photon loop around the muon, the pointlike proton and the composite proton using dipole form factors. Right panel: Zoom in on the proton contribution using dipole form factors as well as the most recent form factors from dispersion theory [5]. The solid and dotted-dashed lines refer to the elastic and elastic plus inelastic contribution.

to Eq. (2), one recognizes that the radiative corrections (i.e. changes of cross-section ratios) from vacuum polarization and soft photon bremsstrahlung are the same for a structureful and structureless proton. Concerning the ratio H_1/H_0, one finds that this feature still holds for the muonic part written in the first line in Eq. (5). To high accuracy this ratio is equal to $2F_1^\gamma$, because the other muon form factor F_2^γ is suppressed by a factor of the muon mass squared, and it enters with a further suppression factor t. Interestingly, the situation is different for the vertex corrections at the proton, described by $G_{E,M}^\gamma$ in the second and third line of Eq. (5). As shown in the left panel of Fig. 7, for a structureless proton[1] one finds that this part of the ratio H_1/H_0 grows from zero to 1.33×10^{-4} in the momentum transfer region $0 < Q < M/2$. If these vertex corrections, as specified by $G_{E,M}^{\gamma\text{-fin}}$, are evaluated with phenomenological form factors, the corresponding radiative correction H_1/H_0 is negative and reaches more significant values of about -0.4%. Further effects from inelastic contributions [modeled here by $\Delta^+(1232)$-resonance excitations] turn out to be of magnitude 10^{-4} and are thus not relevant in view of the experimental accuracy; see the right panel of Fig. 7.

In Fig. 8 we show the radiative corrections from all discussed sources[2] (of order α/π) for the planned AMBER experiment with a muon beam energy of $E_1 = 100$ GeV and an assumed infrared cutoff of $\lambda = 20$ MeV, corresponding to an energy resolution that limits the detection of photons with an energy below 20 MeV. We set $\xi_{ir} = 0$ in order to have all individual contributions independent of

the regulator mass m_γ. At small momentum transfers $Q/M \lesssim 0.06$, vacuum polarization is the most dominant effect, because it is driven by the electron mass scale. After that, the soft photon radiation takes over, with a sizable contribution (of 2%) from the photon-loop form factor $2F_1^{\gamma\text{-fin}}$, involving the muon mass scale, at the upper end of the momentum transfers considered here. The negative photon-loop form factor contribution from the proton stays below 0.4% in magnitude, and the two-photon exchange correction of maximal size 0.3×10^{-4} can essentially be neglected.

As a variation we show in Fig. 9 the radiative corrections for a smaller muon beam energy of $E_1 = 50$ GeV (as it is also planned by AMBER) and the same infrared cutoff of
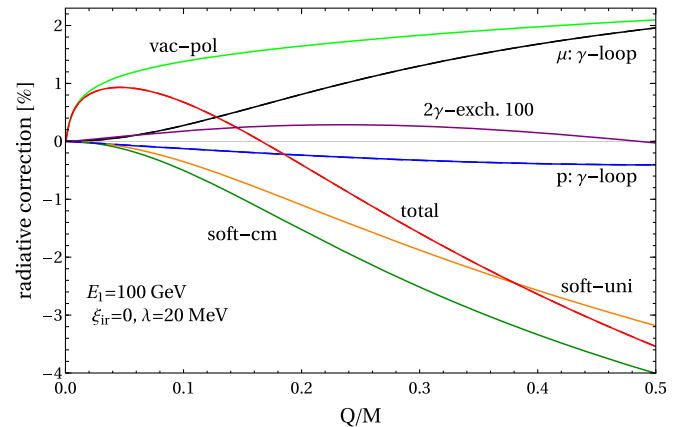

FIG. 8. Radiative corrections for the AMBER kinematics with $E_1 = 100$ GeV. The individual radiative corrections from vacuum polarization, the virtual photon loops and soft bremsstrahlung are shown together with their sum; see the solid line labeled "total".

---

[1] For a pointlike proton one has $G_E^\gamma = F_1^\gamma + tF_2^\gamma/4$ and $G_M^\gamma = F_1^\gamma + F_2^\gamma$ with $F_{1,2}^\gamma$ as in Eqs. (6), (7) setting $r = 1$.

[2] For recent work on two-loop radiative corrections of order $(\alpha/\pi)^2$ to lepton-proton scattering, see Refs. [31,32].
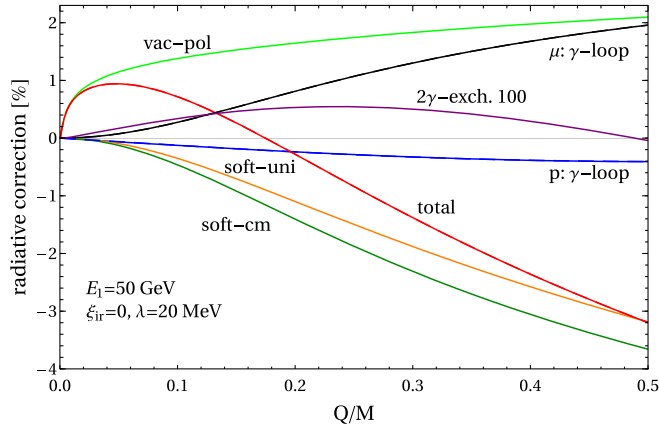
FIG. 9. Radiative corrections for the AMBER kinematics with $E_1 = 50$ GeV. Same notation as in Fig. 8.

$\lambda = 20$ MeV. In comparison to the case with $E_1 = 100$ GeV, one observes an increase of the two-photon exchange correction and some slight changes in the soft photon components, but the overall pattern is nearly the same.

Of equal interest is the pattern of radiative corrections for the MUSE experiment, which measures at much lower muon beam energies $E_1 = 156, 186, 235$ MeV. Our results for the case of $E_1 = 235$ MeV are shown in Fig. 10, choosing an infrared cutoff of $\lambda = 2$ MeV which seems appropriate for the energy resolution of MUSE. The essential differences to Figs. 8, and 9 are (i) that the muonic vertex corrections get slightly reduced by the Pauli form factor F_2^γ and (ii) that the effects from two-photon exchange are strongly enhanced by more than a factor of 100. At the same time, the effects of $\Delta^+(1232)$-resonance excitation are completely negligible for both the 2γ exchange and the electromagnetic vertex corrections at the proton.
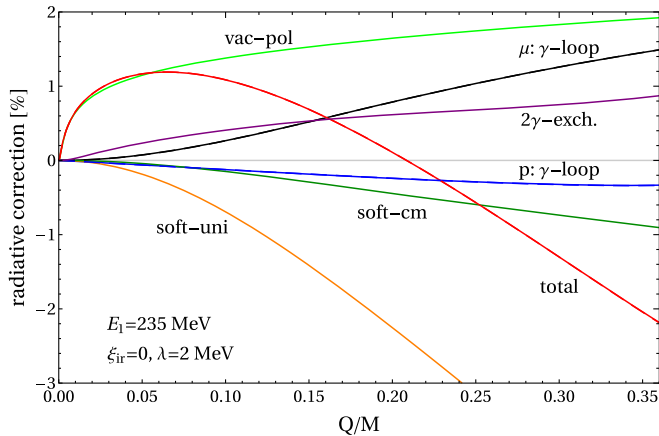

FIG. 10. Radiative corrections for the MUSE kinematics with $E_1 = 235$ MeV. Same notation as in Fig. 8.

VII. SUMMARY AND OUTLOOK

In this work we have systematically calculated the radiative corrections of order α/π to elastic muon-proton scattering. These corrections consist of vacuum polarization, soft photon radiation, photon-loop form factors of the muon and of the proton, and two-photon exchange corrections. The first three components turn out to be universal in the sense that the structure of the proton (as encoded in the electric and magnetic form factors $G_{E,M}$) drops out in the respective ratios to the Born cross section. The photon-loop induced vertex corrections at the proton give rise to additional form factors $G_{E,M}^\gamma \sim \alpha/\pi$, whose infrared finite pieces can be calculated with sufficient accuracy. The elastic contribution to $G_{E,M}^\gamma$ from the proton intermediate state is almost independent of the input form factors into the pertinent triangle diagram, while inelastic contributions [modeled here by excitation of the low-lying $\Delta(1232)$-resonance] play numerically no role for the relevant ratio H_1/H_0. The same is even more true for the two-photon exchange, whose relative effect measured by the ratio H_2/H_0 stays well below 10^{-4} in the small momentum transfer region $Q < 400$ MeV. The latter statement about the marginal role of the 2γ exchange holds for the kinematics of the AMBER experiment with high muon beam energies of $E_1 = 50, 100$ GeV. However, for the MUSE experiment at much lower beam energies $E_1 \sim 200$ MeV the 2γ exchange contributes with ordinary size up to about 1%. In any case, the aspects of proton structure that enter the virtual radiative corrections do not limit the precision of extracting the form factors $G_{E,M}$, and finally the proton radius r_p, accurately from elastic muon-proton scattering.

With the complete radiative corrections of the size of a few percent and aiming for permille accuracy, a prominent role is played by the soft photon radiation. The treatment of undetected soft photon bremsstrahlung in this work in terms of a small momentum sphere $|\vec{\ell}| < \lambda$ in the center-of-mass frame corresponds to an idealized experiment. In a real experiment this region in phase space has a more complicated structure with smooth edges due to varying detector acceptances and other effects. By computing the fivefold differential cross section $d^5\sigma/(d\Omega_\mu d\Omega_\gamma d\omega_\gamma)$ for the process $\mu^\mp p \to \mu^\mp p \gamma$ at tree level, and integrating it over the experimentally "blind regions" (of course, now with exclusion of the small momentum sphere $|\vec{\ell}| < \lambda$) the treatment of undetected soft and hard photon bremsstrahlung can be tailored to the specific experimental conditions. At the same time this fivefold differential cross section can be used for experimental verification of its spectral and angular distributions in regions where additional photons are detectable. Work along these lines in collaboration with members of the AMBER collaboration is in progress. In passing we note that our formalism applies in the same way to $e^\mp p$ scattering by setting $r = 2.966 \times 10^{-7}$. One just

keeps very small terms that are usually dropped in an expansion up to leading logarithms plus constants.

ACKNOWLEDGMENTS

[1] S. Bifani, S. Descotes-Genon, A. Romero Vidal, and M. H. Schune, J. Phys. G **46,** 023001 (2019).

[2] E. J. Downie (MUSE Collaboration), EPJ Web Conf. **73,** 07005 (2014).

[3] B. Adams *et al.*, arXiv:1808.00848.

[4] R. Pohl, R. Gilman, G. A. Miller, and K. Pachucki, Annu. Rev. Nucl. Part. Sci. **63,** 175 (2013).

[5] Y. H. Lin, H. W. Hammer, and U.-G. Meißner, Phys. Rev. Lett. **128,** 052002 (2022).

[6] Y. H. Lin, H. W. Hammer, and U.-G. Meißner, Eur. Phys. J. A **57,** 255 (2021).

[7] R. Pohl *et al.*, Nature (London) **466,** 213 (2010).

[8] H. Fleurbaey, S. Galtier, S. Thomas, M. Bonnaud, L. Julien, F. Biraben, F. Nez, M. Abgrall, and J. Guéna, Phys. Rev. Lett. **120,** 183001 (2018).

[9] N. Bezginov, T. Valdez, M. Horbatsch, A. Marsman, A. C. Vutha, and E. A. Hessels, Science **365,** 1007 (2019).

[10] A. Grinin, A. Matveev, D. C. Yost, L. Maisenbacher, V. Wirthl, R. Pohl, T. W. Hänsch, and T. Udem, Science **370,** 1061 (2020).

[11] A. D. Brandt, S. F. Cooper, C. Rasor, Z. Burkley, D. C. Yost, and A. Matveev, Phys. Rev. Lett. **128,** 023001 (2022).

[12] W. Xiong *et al.*, Nature (London) **575,** 147 (2019).

[13] A. Gasparian *et al.* (PRad Collaboration), arXiv:2009.10510.

[14] A. Denig, J. Univ. Sci. Tech. China **46,** 608 (2016).

[15] N. Kaiser, J. Phys. G **37,** 115005 (2010).

[16] N. Kaiser, J. Phys. G **44,** 055003 (2017).

[17] O. Tomalak and M. Vanderhaeghen, Eur. Phys. J. C **76,** 125 (2016).

[18] O. Tomalak and M. Vanderhaeghen, Eur. Phys. J. C **78,** 514 (2018).

[19] C. Peset, A. Pineda, and O. Tomalak, Prog. Part. Nucl. Phys. **121,** 103901 (2021).

[20] X. H. Cao, Q. Z. Li, and H. Q. Zheng, arXiv:2112.06230.

[21] S. Actis *et al.* (Working Group on Radiative Corrections and Monte Carlo Generators for Low Energies), Eur. Phys. J. C **66,** 585 (2010).

[22] J. Arrington, P. G. Blunden, and W. Melnitchouk, Prog. Part. Nucl. Phys. **66,** 782 (2011).

[23] W. Albrecht *et al.*, Nucl. Phys. **B27,** 615 (1971); **B30,** 642 (1971).

[24] S. Galster, G. Hartwig, H. Klein, J. Moritz, K. H. Schmidt, W. Schmidt-Parzefall, D. Wegener, and J. Bleckwenn, Phys. Rev. D **5,** 519 (1972).

[25] V. Burkert and Z. J. Li, Phys. Rev. D **47,** 46 (1993).

[26] M. Benmerrouche, R. M. Davidson, and N. C. Mukhopadhyay, Phys. Rev. C **39,** 2339 (1989).

[27] I. T. Lorenz, U.-G. Meißner, H. W. Hammer, and Y. B. Dong, Phys. Rev. D **91,** 014023 (2015).

[28] P. G. Blunden and W. Melnitchouk, Phys. Rev. C **95,** 065209 (2017).

[29] O. Tomalak and M. Vanderhaeghen, Eur. Phys. J. A **51,** 24 (2015).

[30] L. C. Maximon and J. A. Tjon, Phys. Rev. C **62,** 054320 (2000).

[31] R. D. Bucoveanu and H. Spiesberger, Eur. Phys. J. A **55,** 57 (2019).

[32] P. Banerjee, T. Engel, A. Signer, and Y. Ulrich, SciPost Phys. **9,** 027 (2020).